Research Article | Vol. 29, No. 5 / 1 March 2021 / Optics Express 6714

Optics EXPRESS

Diving angle optimization of BRF in a single-frequency continuous-wave wideband tunable titanium:sapphire laser

JIAO WEI,[1] XUECHEN CAO,[1] PIXIAN JIN,[1,2] JING SU,[1,2] HUADONG LU,[1,2,*] AND KUNCHI PENG[1,2]

[1]*State Key Laboratory of Quantum Optics and Quantum Optics Devices, Institute of Opto-Electronics, Shanxi University, Taiyuan 030006, China*
[2]*Collaborative Innovation Center of extreme Optics, Shanxi University, Taiyuan 030006, China*
[*]*luhuadong@sxu.edu.cn*

Abstract: In this study, the optimal condition of a multi-plate birefringent filter (BRF) used in a single-frequency continuous-wave (CW) tunable laser is theoretically and experimentally investigated. The dependence of the optimal condition on the diving angle of the BRF optical axis is first deduced. Based on the proposed optimal condition, the diving angle of the BRF optical axis is optimized to 29.1°. Subsequently, a novel off-axis multi-plate BRF with a thickness ratio of 1:2:5:9 and the thinnest plate of 0.5 mm is designed and utilized in a tunable titanium:sapphire (Ti:S) laser. As a result, the operating wavelength of the Ti:S laser is successfully tuned from 691.48 to 995.55 nm by rotating the BRF 18°. The obtained tuning slope efficiency and maximum tuning range are 16.9 nm/° and 304.07 nm, respectively. The experimental results agree well with the theoretical analysis results, which provide a feasible approach for designing BRFs to satisfy the requirements of other single-frequency CW wideband tunable lasers.

© 2021 Optical Society of America under the terms of the OSA Open Access Publishing Agreement

1. Introduction

All-solid-state single-frequency continuous-wave (CW) tunable lasers [1] has been applied in many fields owing to its intrinsic advantages of low intensity noise, perfect beam quality, high stability, and broad tuning range [2]. In particular, the single-frequency CW wideband tunable titanium:sapphire (Ti:S) laser has played important roles in atom cooling and trapping [3,4], atomic clocks [5], and precise measurements [6] because its operating wavelengths of 700-1000 nm cover the transition lines of kalium (K), rubidium (Rb) and cesium (Cs) atoms. As initial laser source, it is used to generate three-color entanglement at optical fiber communication and atomic storage wavelengths, which can be used to build the quantum internet [7]. With the assistance of frequency up-conversion and down-conversion, their laser wavelengths can be extended to deep-ultraviolet [8,9] and mid-infrared [10,11] regions. From Yarborough inserted a quartz birefringent filter (BRF) in a laser cavity at the Brewster angle to achieve laser wavelength tuning in 1973 [12], the BRF had become the most popular candidate to realize the wavelength tuning of a laser [13]. At first, the optical axis of the adopted BRF often lay on the surface of the BRF plate. Using these kinds of BRFs, Bloom and Holton et al. studied the nature of the eigenmodes of a laser resonator with a BRF and designed a BRF for high-power dye lasers in 1974, respectively [14,15]. In 1980, Preuss and Gole further experimentally developed a three-stage BRF for smoothly tuning over the visible region based on the theoretical analysis [16]. It was worth mentioning that Holtom also presented that the BRF with tilted angle of the optical axis was benefit to effectively increase the tuning slope efficiency by comparing the off-axis BRF to that with the optical axis parallel to the surface, which paved a good way to broaden the tuning range of the BRF. Subsequently, lots of methods for optimizing the off-axis BRF were developed [17]. Especially, Naganuma et al. developed a variable bandwidth off-axis single-plate

#419580 https://doi.org/10.1364/OE.419580
Journal © 2021 Received 12 Jan 2021; revised 5 Feb 2021; accepted 10 Feb 2021; published 17 Feb 2021

Optics EXPRESS

BRF for tunable femtosecond lasers in 1992. By optimizing the optical axis diving angle of quartz crystal quartz to 66°, 2-octave tuning range or a 4-times variable bandwidth were achieved [18]. On this basis, an off-axis magnesium fluoride BRF for smoothly tuning of broadband lasers was reported by Demirbas in 2017. To this day, the BRF made of different materials had been developed and broadly utilized in various kinds of tunable lasers [19–21]. However, for the BRF used in the single-frequency CW tunable laser, except the broad tuning range, the attained laser linewidth and sidebands rejection ability while tuning also had to be considered [22]. In this case, compared to single-plate BRF, multi-plate BRF became more important. Although Wang and Yao analyzed the transmitted and tuning characteristics of off-axis multi-plate BRF and pointed out that the four-plate BRF designed with thickness ratio of 1:2:4:9 or 1:2:5:9 had maximum blocking from the side transmission peaks [23], there was no literature to further optimize the optical axis diving angle of the BRF to the best of our knowledge. Actually, after the thickness ratio of multi-plate BRF and thicknesses of BRF plates were determined, it was necessary to look for the optimal optical axis diving angle of the adopted BRF to cover the florescence spectrum of the gain medium. In order for this purpose, we developed an optimal condition for a multi-plate BRF suitable for the single-frequency CW tunable laser by considering the fluorescent spectral range of the laser medium in this paper. According to the proposed optimal condition, the diving angle of the BRF optical axis was optimized to 29.1° when the Ti:S crystal acted as the laser medium. On this basis, a novel off-axis multi-plate BRF with a thickness ratio of 1:2:5:9 and the thinnest plate of 0.5 mm was designed and utilized in a tunable Ti:S laser. As a result, the operating wavelength of the Ti:S laser was successfully tuned from 691.48 to 995.55 nm by rotating the BRF of 18°. The obtained tuning slope efficiency and maximum tuning range were as large as 16.9 nm/° and 304.07 nm, respectively.

2. Theoretical analysis

When a quartz crystal is used as the tuning element for a tunable laser, it is placed in the resonator at the Brewster angle and every parameter of the adopted BRF can be described according to Fig. 1. $\sum(k)$ perpendicular to the surface of the crystal represents the incident plane, where both incident and refracted rays lie on, and θ_i and θ_r are the incident and refracted angles, respectively. ($\overline{OC}$) represents the optical axis and α is named the angle between $\overline{OC}$ and the BRF surface. Therefore, the projection $\overline{OD}$ on the crystal surface is obtained. The angle between $\overline{OD}$ and $\overline{QD}$ is termed tuning angle A, and we can define the starting point A=0° while $\overline{OD}$ and $\overline{QD}$ coincident. In order to calculate the phase difference between the generated ordinary (o) and extraordinary (e) lights, the angle (γ) between the refractive ray and the optical axis is introduced. In addition, to satisfy the tuning requirements of the single-frequency CW tunable laser, the BRF often designed as multi-plate structure, where the thinnest and thickest plates decide the tuning range and tuning precision, respectively. In particular, for the traditional BRF, if we expect that the tuning range can cover the fluorescence spectrum of the Ti:S crystal (700-1000 nm), the thinnest plate has to be as thin as 0.09 mm, which results in low tuning slope efficiency, tuning processing difficulty and frangibility. At the same time, according to the information applied by Ref. [18], the thickness ratio 1:2:5:9 of the quartz BRF is the best choice for the single-frequency tunable laser owing to its good sideband-rejection ability. Therefore, considering the processing and durability, the thinnest plate and thickness ratio of 0.5 mm and 1:2:5:9, respectively, are adopted in the experiment to design the broadband tuning element, and the designed BRF is depicted in Fig. 2. The diameters of the four plates and spacings between them are customized as 25.2 mm and 0.5 mm, respectively. In this case, it is expected that the tuning range of the designed off-axis multi-plate BRF can basically cover the fluorescence spectrum of the Ti:S crystal by optimizing the diving angle of optical axis.

Optics EXPRESS

According to the polarizing interference tuning theory, the wavelength transmission of the multi-plate BRF is expressed as,

$$T(\delta_i) = \prod_{i=1}^{i=n}[1 - \sin^2(2\varphi)\sin^2(\frac{\delta_i}{2})], \tag{1}$$

where φ is the angle between the incident plane and the electric displacement vector of refractive light and determined by the following equation,

$$\sin\varphi = \cot\gamma(\tan\theta_i - \frac{\sin\alpha}{\cos\theta_i\cos\gamma}), \tag{2}$$

δ_i is the phase difference of the ith quartz crystal, and n is the plate number of the multi-plate quartz BRF. Focusing on Eq. (1), only if $\sin^2(2\varphi)$ or $sin^2(\delta_i/2)$ is equal to zero, $T(\delta_i)$ is equal to unity, and the output wavelength loss of zero for transmission of laser was obtained accordingly. For $\sin^2(2\varphi) = 0$ inevitably leads to $T(\delta_i)$ of unity for all wavelengths and does not give rise to frequency selectivity. $sin^2(\delta_i/2) = 0$ is the best choice to ensure the wavelength selection ability and the maximum transmission for output wavelength of the designed BRF. In this case, $\delta_i = 2k\pi$ (k=±1, ±2,. . .). On contrary, T(φ, δ_i) is equal to $1 - \sin^2(2\varphi)$, which represents the minimum transmission of the single-plate BRF. Therefore, it is necessary to introduce parameter D to represent the ability of sideband suppression. And D is defined as the ratio of the maximum and minimum transmission and expressed as follows,

$$D(\varphi, \delta_i) = \frac{T_{max}(\varphi, \delta_i)}{T_{min}(\varphi, \delta_i)} = \frac{1}{1 - \sin^2(2\varphi)}. \tag{3}$$

Additionally, the operating wavelength λ is decided by γ and expressed as,

$$\lambda = \frac{d(n_o - n_e)\sin^2\gamma}{k\sin\theta_i}, \tag{4}$$

where k is the interference order, d is the thickness of the thinnest plate and chosen to be 0.5 mm in the experiment, and n_o-n_e is the index difference between the o and e rays.

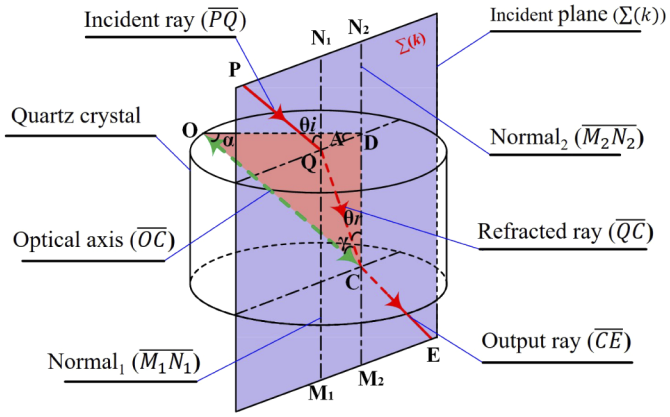


Fig. 1. Schematic diagram of single-plate BRF.

Combining Eqs. (1)–(4), it can be inferred that parameter D is related to α and λ. And we can improve D by optimizing the diving angle of optical axis to make $\sin 2\varphi$ closer to unity in

Optics EXPRESS

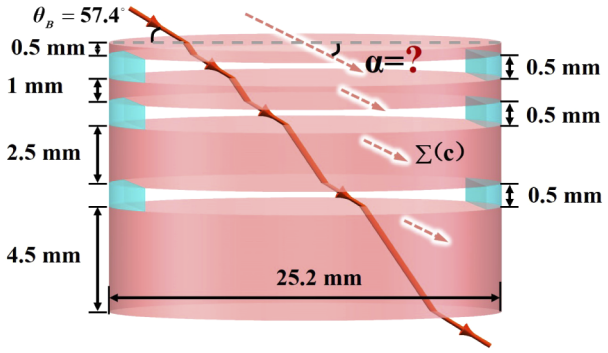


Fig. 2. Diagram of designed four-plate BRF.

the desired wavelength tuning range. As a result, the optimal condition of the BRF is obtained, which is expressed as,

$$D(\alpha, \lambda_{max}) = D(\alpha, \lambda_{min}), \tag{5}$$

where λ_{max} and λ_{min} are the upper and lower limits for the fluorescence spectrum of the gain crystal, respectively. For the Ti:S crystal with the fluorescence spectrum of 700-1000 nm, the relationship between $\sin 2\varphi$ and α is simulated and depicted in Fig. 3. Clearly, the optimal value of α for λ=700 nm is 31.7° because the value of $\sin 2\varphi$ is equal to unity and the corresponding value of D is maximum. With the increase of the wavelength, the optimal value of α dramatically decreases. When the wavelength increases to 1000 nm, the corresponding optimal α decreases to 25.3°. A critical point satisfies the optimal condition in Eq. (5), which is termed Q in Fig. 3. For point Q, the value of α is 29.1°, and the value of $\sin 2\varphi$ is closest to the maximum of unity for the wavelength range of 700-1000 nm. Therefore, α=29.1° is the optimal condition for the BRF in the wideband single-frequency CW tunable Ti:S laser. Actually, if the tuning range over 300 nm was desired, we just need to further optimize the diving angle depending on the optimal condition we developed.

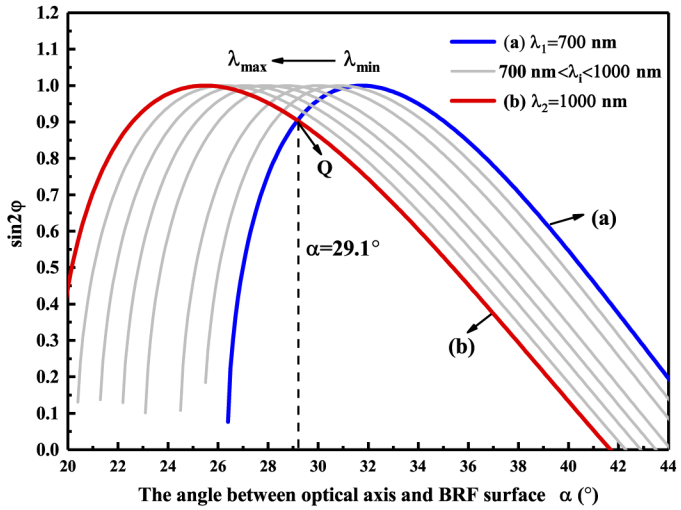


Fig. 3. Relationship between $\sin 2\varphi$ and α corresponding to different wavelengths (700-1000 nm).

Optics EXPRESS

Subsequently, to reveal the superiority of the designed off-axis multi-plate BRF with the optimal diving angle, the tuning ability for α=0° and α=29.1° are compared and investigated, and the calculated results are illustrated in Fig. 4. As plotted in Fig. 4(a), when α is equal to 0°, the resonant wavelengths are located in the range of 700-1000 nm for k=4, 5, and 6. However, there is no tuning curve to directly cover the fluorescence spectrum of the Ti:S crystal (700-1000 nm). Moreover, there is a large wavelength overlap between the tuning curves of different interference orders, which is likely to cause mode-hopping in the tuning process. Even without considering the mode-hopping for k=5, which has a broadest wavelength range of 246 nm, the BRF must be rotated by 62° to achieve the goal. The corresponding tuning slope efficiency is only 4.0 nm/°. By contrast, in Fig. 4(b), when α is equal to 29.1°, all of the tuning curves in the plotted range can cover the wavelength of 700-1000 nm. In particular, the overlap of the tuning curves is inexistence in k=2, 3, and 4, which is greatly beneficial for a smooth wavelength tuning. In addition, for k=2, the BRF can easily cover the tuning range of 700-1000 nm only by changing

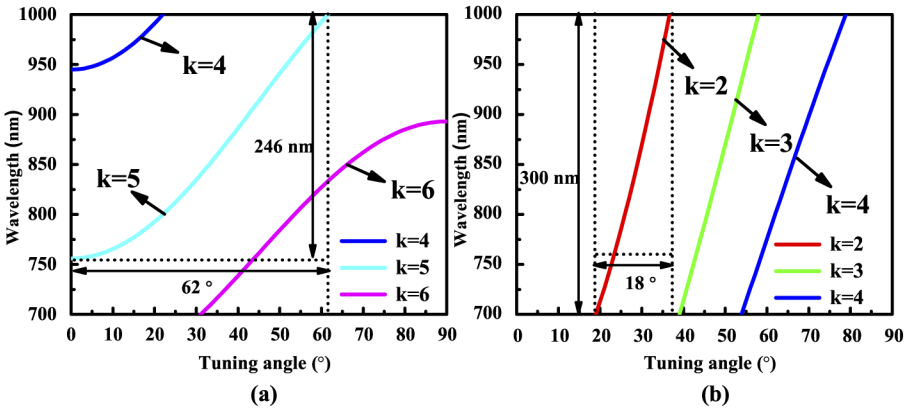


Fig. 4. Tuning curves of the BRF for α=0° and α=29.1°.

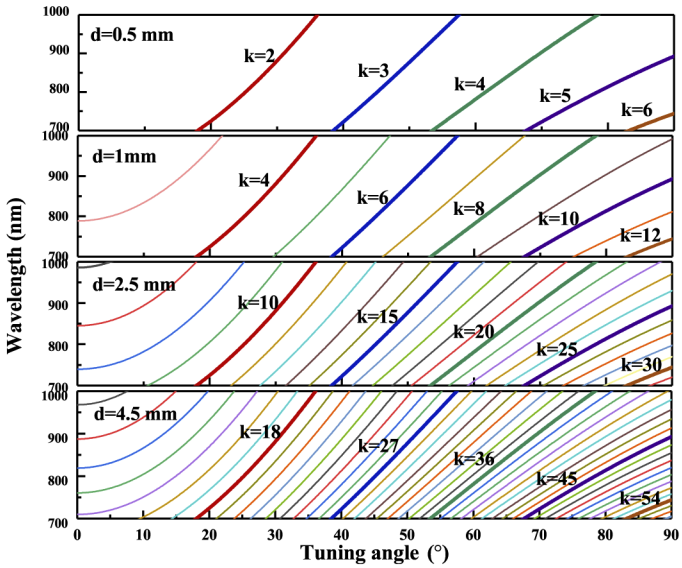


Fig. 5. Theoretical simulation of tuning curves of designed four-plate BRF.

Optics EXPRESS

the tuning angle of 18°. The corresponding tuning slope efficiency is up to 16.7 nm/°, which is much larger than that of k=5 shown in Fig. 3(a).

Furthermore, after the parameters of the BRF are determined, the tuning curves of the designed four-plate off-axis BRF are simulated and shown in Fig. 5. For the thinnest plate, no more than two wavelengths can lase depending on the value of A in the plotted range of 700-1000 nm. For the thickest plate, more than ten wavelengths can lase in the plotted range owing to the dense interference orders. In addition, some of the lines have been emphasized for their identical shape and location. It is obvious that the free spectral range (FSR) is inversely proportional to the thickness of the plate. Meanwhile, the transmission curves of the designed four-plate BRF are simulated and the results are shown in Fig. 6. It is seen that the linewidth of the composite transmission curve is effectively narrowed when all four plates are used together as a four-plate

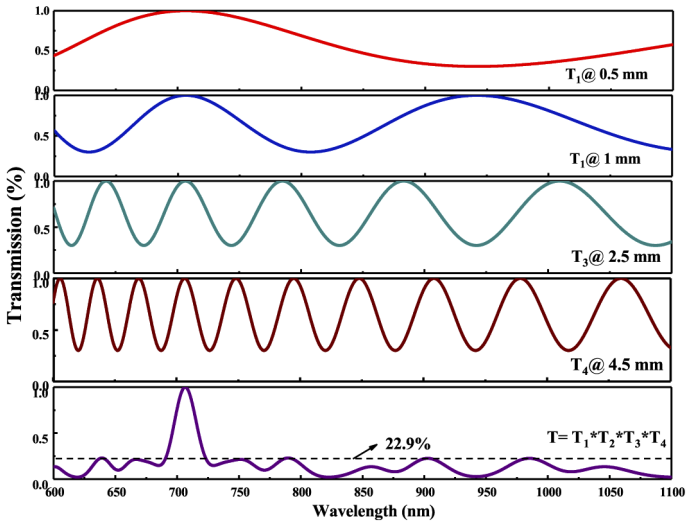


Fig. 6. Theoretical simulation of transmission curves of designed four-plate BRF.

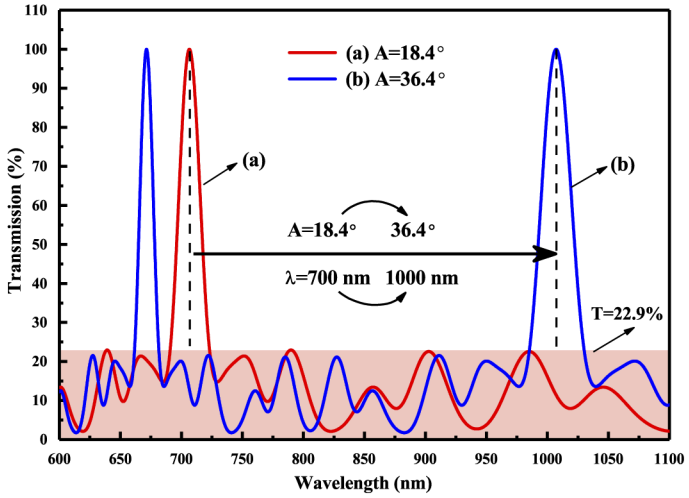


Fig. 7. Transmission curve of designed BRF when tuning angle A varies from 18.4° to 36.4°.

Optics EXPRESS

BRF, and the transmission of the sidebands are always below 22.9%. When the tuning angle A varies from 18.4° to 36.4°, the operating wavelength is tuned from 700 nm to 1000 nm, which is shown in Fig. 7. It is proven that the spacings between two neighboring main transmission peaks are as large as 300 nm, and the sidebands will not lase easily because their transmittances are always below 22.9%. Therefore, the designed BRF can well satisfy the smooth tuning of 300 nm in the wideband single-frequency CW tunable Ti:S laser.

3. Experimental setup

Based on the newly designed BRF, a wideband single-frequency CW tunable Ti:S laser with a unidirectional ring cavity was built and illustrated in Fig. 8. A homemade all-solid-state single-frequency CW 532 nm laser [24–26] with a maximum radiation power of 13.8 W acted as the pump source. The pump laser beam was collimated by a lens f_1 with a focal length of 200 mm and focused onto the Ti:S crystal by another lens f_2 with a focal length of 120 mm for mode matching. The incident angle of f_2 was 7.9° to compensate for the astigmatism of the pump laser in the Ti:S crystal owing to the Brewster incident angle. The Ti:S resonator had a bow-tie-type ring configuration with two spherical mirrors M_1 and M_2 (curve radius of 100 mm) and two plane mirrors M_3 and M_4. The input coupler M_1 was coated with high transmission (HT) and high reflection (HR) films for 532 and 680-1030 nm, respectively. Both M_2 and M_3 were coated with the HR film for 680-1030 nm. With the assistance of the intracavity loss measurement method [27], the measured intracavity loss was 4.5%. In this case, the transmission of the output coupler M_4 was optimized to 5.5% for the 680-1030 nm laser. The incident angles of the cavity mirrors M_1 and M_2 were 19.4°, which well compensated for the astigmatism caused by the intracavity Brewster-cut elements including the Ti:S crystal, BRF, and terbium gallium garnet (TGG). The Ti:S crystal (GT Advanced Technologies) was 20 mm long and cut at a Brewster angle relative to the c-axis of the crystal. The figure-of-merit, defined by residual absorption at 532 and 800 nm, exceeded 375, and the nominal Ti^{3+} doping concentration was 0.05 wt.%. The Ti:S crystal was mounted in a closed copper block oven and surrounded by cooling circulation water, whose temperature was controlled at 15 °C with an accuracy of ±0.1 °C. Subsequently, the copper block oven was placed at the waist between M_1 and M_2 to obtain a high pump rate. The optimized off-axis four-plate BRF was mounted on a rotating electrical machine (AG-PR100, Newport) and inserted at the Brewster angle into the cavity to implement wavelength tuning. A dispersion-compensated optical diode was utilized to ensure the unidirectional operation of the Ti:S laser, which was composed of a Brewster-cut (62.9°) 2-mm-long TGG Faraday crystal

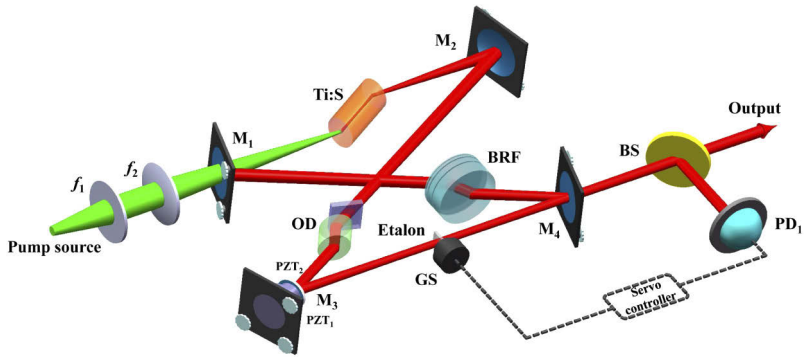


Fig. 8. Schematic diagram of designed Ti:S laser. f_1 and f_2: coupling lenses; Ti:S: titanium:sapphire crystal; OD: optical diode; BRF: birefringent filters; PZT_1: long piezoelectric transducer; PZT_2: short piezoelectric transducer; GS: galvanometer scanner; BS: beam splitter; PD_1: photodetector.

Optics EXPRESS

surrounded by a stack of permanent Sm-Co ring magnet with a magnetic field intensity of 68 Gs and a thin quartz plate exhibiting a natural optical rotation with a thickness of 0.342 mm. In addition, a 0.5-mm-thick fused silica etalon coated with 20% reflective film for 680-1030 nm was directly installed on the spindle of a galvanometer scanner and inserted into the resonator to realize finely frequency tuning. Two piezoelectric transducers with lengths of 25 mm (PZT_1) and 9 mm (PZT_2) were successively glued to M_3 to finely scan and lock the cavity length.

4. Experimental results

The tuning characteristic was firstly investigated in the experiment. In this regard, a small portion of the output laser was injected into a grating spectrograph (Maya2000 Pro, Ocean Optics) to precisely read the operating wavelength of the Ti:S laser. The remainder was injected into a power meter (PM30, Coherent Co., Ltd.) to record the corresponding power. The results are illustrated in Fig. 9. Clearly, the wavelength of the output laser was tuned from 691.48 nm to 995.55 nm with the BRF rotation angle of 18°. The obtained wavelength tuning range covered the fluorescence spectrum of the Ti:S crystal (700-1000 nm). The experimental results were in good agreement with the theoretical analysis results, which revealed that the newly designed BRF based on the presented optimal condition satisfied the requirement of a wideband wavelength tuning for the Ti:S laser. The obtained wavelength could cover the transition lines of K (D_2, 2.48 W @ 767 nm; D_1, 2.60 W @ 770 nm), Rb (D_2, 2.46 W @ 780 nm; D_1, 2.18 W @ 795 nm) and Cs atoms (D_2, 2.35 W @ 852 nm; D_1, 2.11 W @ 895 nm) [28]. In addition, the obtained 756 nm laser (2.40 W), 820 nm laser (2.65 W), 902 nm laser (1.96 W) and 911 nm laser (1.84 W) could be frequency-doubled to 378 nm [29], 410 nm, 451 nm [30,31] and 455.5 nm [32] to excite atoms into excited states, and further satisfy the experimental requirements in various fields.

On this basis, the resonant wavelength was tuned to 795 nm by rotating the BRF to precisely match the D_1 transition lines of the Rb atoms. After the intracavity etalon was successfully locked to the resonant longitudinal mode of the Ti:S laser with the assistance of the direct modulation-locking technology [33], the stable single-longitudinal-mode (inset of Fig. 10) was easily observed by a homemade Fabry-Perot interferometer (F-P-100, Yuguang Co., Ltd.) with a free spectrum range and finesse of 750 MHz and 100, respectively. The long-term power stability was measured and illustrated in Fig. 10. The peak-to-peak fluctuation was less than ±2.2% in 8 h. At the same time, a small portion laser beam was used to measure the transverse-mode

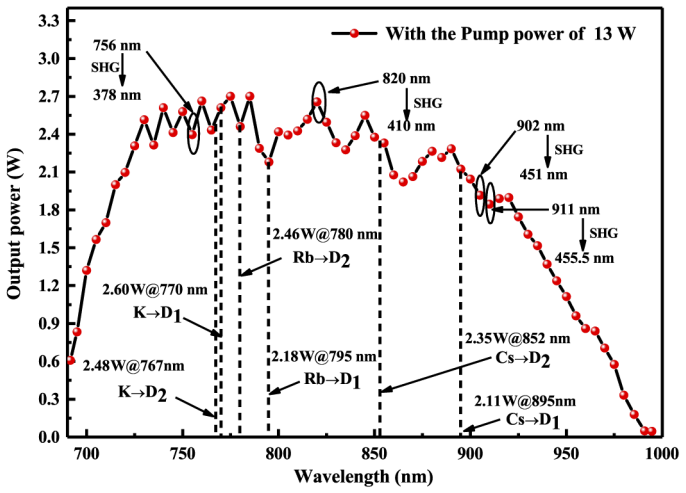


Fig. 9. Measured maximum tuning range of single-frequency CW Ti:S laser.

Optics EXPRESS

characteristics of the achieved Ti:S laser using an M^2 beam quality analyzer (M2SETVIS, Thorlabs), and the results are illustrated in Fig. 11. The measured beam quality was M_x^2=1.02 and M_y^2=1.00, respectively. As shown in the inset of Fig. 11, the output laser beam closely resembled the standard Gauss distribution, which benefited from the favorable astigmatism compensation by optimizing the cavity structure. Subsequently, the linewidth of the achieved Ti:S laser was measured by a frequency beating system with the resolution of 30 kHz. The output laser beam of the Ti:S laser was interfered with that of another similar reference tunable Ti:S laser, whose oscillating frequency was locked to the D_1 transition line of Rb^{87} atoms. Then, the resulting interferometric signal was analyzed by a spectrum analyzer and the measured data are shown in Fig. 12. It was indicated that the linewidth of the achieved Ti:S laser with the etalon locked

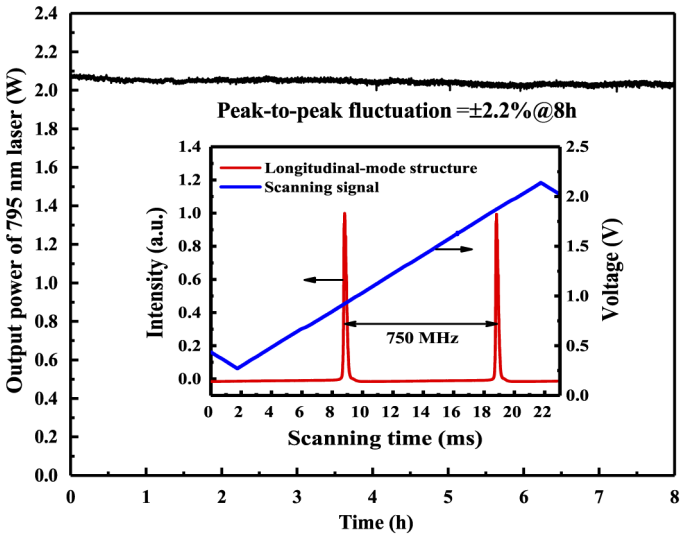


Fig. 10. Long-term power stability of 795 nm laser (the inset is the measured longitudinal-mode structure of Ti:S laser).

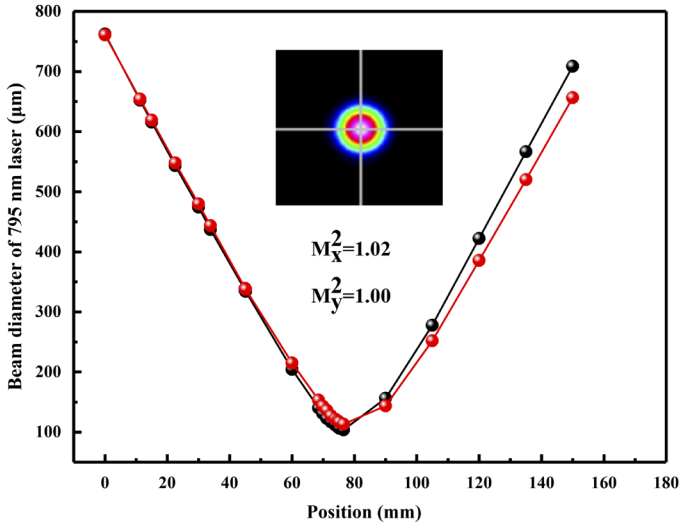


Fig. 11. Measured M^2 value and spatial beam profile of 795 nm laser.

Optics EXPRESS

was 325 kHz, which was much narrower than that of the Ti:S laser without BRF (1.5 nm). Subsequently, by changing the voltage uploaded on the PZT_1 attached to M_3 to scan the cavity length, the operating wavelength of the Ti:S laser varied from 794.945 nm to 795.030 nm, and the maximum continuous frequency-tuning range of 40.3 GHz was attained, as illustrated in Fig. 13. Finally, we successfully locked the resonant longitudinal mode of the obtained Ti:S laser to one of the D_1 transition lines of Rb^{85} through the polarization spectroscopy technology [34–36], which proved that the obtained wideband single-frequency CW tunable Ti:S laser can well match the transition lines of atoms.

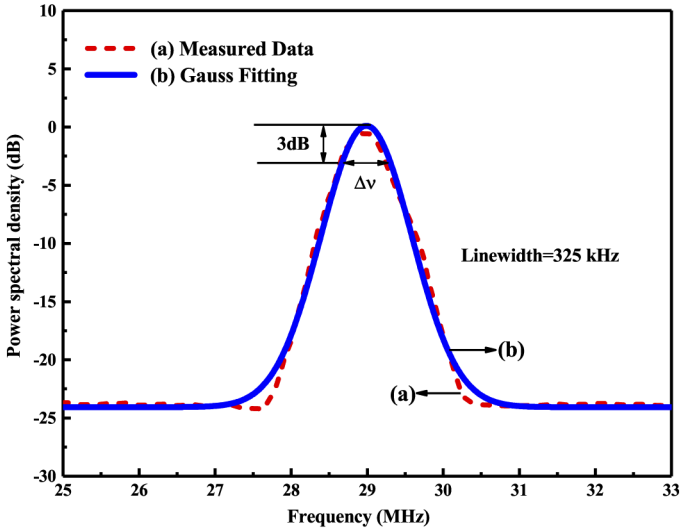


Fig. 12. Measured linewidth data of 795 nm laser by the beat technology and the Gaussian function fitting result.

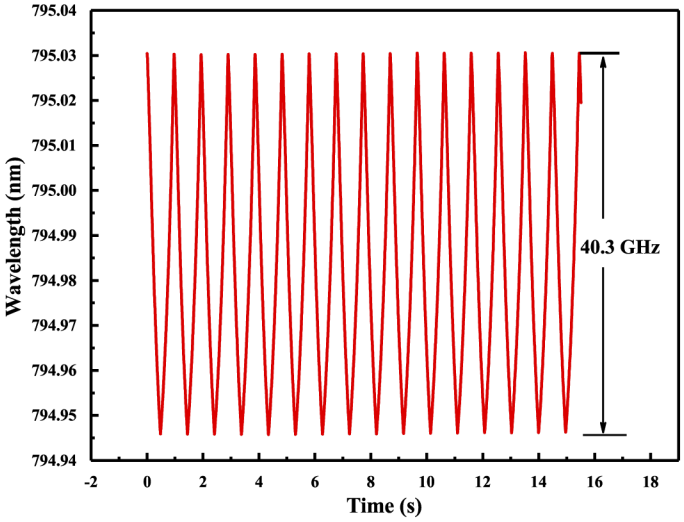


Fig. 13. Continuous frequency-tuning characteristic of Ti:S laser.

Optics EXPRESS

5. Conclusions

The optimal condition of a multi-plate BRF used in CW single-frequency tunable laser was theoretically and experimentally investigated in this study. The dependence of the optimal condition on the diving angle of the BRF optical axis was first deduced. Based on the proposed optimal condition, the diving angle of the BRF optical axis was optimized to 29.1°. Subsequently, a novel off-axis multi-plate BRF with a thickness ratio of 1:2:5:9 and the thinnest plate of 0.5 mm was designed and utilized in a tunable Ti:S laser. Finally, the operating wavelength of the Ti:S laser was successfully tuned from 691.48 to 995.55 nm by rotating the BRF of 18°, which covered the tuning range of 304.07 nm. The obtained tuning slope efficiency and maximum tuning range were as large as 16.9 nm/° and 304.07 nm, respectively. The experimental results were consistent with the theoretical analysis results. It was noteworthy that the whole tuning process was in the same interference order and free of realignment compared to the traditional single-frequency CW tunable Ti:S laser. The presented optimal condition of the BRF could also be used to optimize the BRF of other single-frequency CW wideband tunable lasers. The obtained Ti:S laser system with wideband tuning range and high frequency stability preferably met the requirements of atomic physics, including atom trapping and cooling, atomic clocks, and quantum information storage.

Funding. National Natural Science Foundation of China (61975100, 62027821); National Key Research and Development Program of China (2016YFA0301401); Key Research and Development Program of Shanxi Province (201903D111001); Shanxi "1331 Project" Key Subjects Construction; Program for the Innovative Talents of Higher Education Institution of Shanxi; Shanxi Provincial Graduate Innovation Project (2020SY060).

Disclosures. The authors declare no conflicts of interest.

References

1. Y. Sun, H. D. Lu, and J. Su, "Continuous-wave, single-frequency, all-solid-state Ti:Al_2O_3 laser," Acta Sin. Quant. Opt. **14**(3), 344–347 (2008).
2. P. F. Moulton, "Spectroscopic and laser characteristics of Ti:Al_2O_3," J. Opt. Soc. Am. B **3**(1), 125–133 (1986).
3. T. Kuwanmoto, K. Honda, Y. Takahashi, and T. Yabuzaki, "Magneto-optical trapping of Yb atoms using an intercombination transition," Phys. Rev. A **60**(2), R745–R748 (1999).
4. Z. X. Xu, W. Y. Wu, L. Tian, L. R. Chen, Z. Y. Zhang, Z. H. Yan, S. J. Li, and H. Wang, "Long lifetime and high-fidelity quantum memory of photonics polarization qubit by lifting zeeman degeneracy," Phys. Rev. Lett. **111**(24), 240503 (2013).
5. Z. W. Barber, C. W. Hoyt, C. W. Oates, and L. Hollberg, "Direct excitation of the forbidden clock transition in neutral ^{1}74Yb Atoms confined to an optical lattice," Phys. Rev. Lett. **96**(8), 083002 (2006).
6. F. Wolfgramm, A. Cere, F. A. Beduini, A. Predojevic, M. Koschorreck, and M. W. Mitchell, "Squeezed-light optical magnetometry," Phys. Rev. Lett. **105**(5), 053601 (2010).
7. X. J. Jia, Z. H. Yan, Z. Y. Duan, X. L. Su, H. Wang, C. D. Xie, and K. C. Peng, "Experimental realization of three-tolor entanglement at optical fiber communication and atomic storage wavelengths," Phys. Rev. Lett. **109**(25), 253604 (2012).
8. H. D. Lu, J. Wei, Y. X. Wei, J. Su, and K. C. Peng, "Generation of high-power single-frequency 397.5 nm laser with long lifetime and perfect beam quality in an external enhancement-cavity with MgO-doped PPSLT," Opt. Express **24**(21), 23726–23734 (2016).
9. H. Tomizawa, T. Sato, K. Ogawa, K. Togawa, T. Tanaka, T. Hara, M. Yabashi, H. Tanaka, T. Ishikawa, T. Togashi, S. Matsubara, Y. Okayasu, T. Watanabe, E. J. Takahashi, K. Midorikawa, M. Aoyama, K. Yamakawa, and S. Owada, "Stabilization of a high-order harmonic generation seeded extreme ultraviolet free electron laser by time-synchronization control with electro-optic sampling," High Power Laser Sci. Eng. **3**(2), e14–24 (2015).
10. C. Xi, P. Wang, X. Li, and Z. J. Liu, "Highly efficient continuous-wave mid-infrared generation based on intracavity difference frequency mixing," High Power Laser Sci. Eng. **7**(5), e67–71 (2019).
11. J. Mandon, E. Sorokin, I. T. Sorokina, G. Guelachvili, and N. Picque, "Supercontinua for high-resolution absorption multiplex infrared spectroscopy," Opt. Lett. **33**(3), 285–287 (2008).
12. J. M. Yarborough and J. L. Hobart, *Conference on Laser Engineering and Application* (Optical Socity of America, Washington, DC, (1973), postdeadline paper XX.
13. Z. X. Lu, D. Q. Tang, H. Z. Hu, and W. Liu, "Synthetical design of tunable birefringent filters for Ti:sapphire laser," J. Optoelec. Laser **10**, 498 (1999).
14. A. L. Bloom, "Modes of a laser resonator containing tilted birefringent plates," J. Opt. Soc. Am. **64**(4), 447–452 (1974).

Optics EXPRESS

15. G. Holtom and O. Teschke, "Design of a Birefringent Filter for High-Power Dye Lasers," IEEE J. Quantum Electron. **10**(8), 577–579 (1974).
16. D. R. Preuss and J. L. Gole, "Three-stage birefringent filter tuning smoothly over the visible region: theoretical treatment and experimental design," Appl. Opt. **19**(5), 702–710 (1980).
17. S. Lovold, P. F. Moulton, D. K. Killinger, and N. Menyuk, "Frequency tuning characteristics of a Q-Switched Co:MgF_2 laser," IEEE J. Quantum Electron. **21**(3), 202–208 (1985).
18. K. Naganuma and G. Lenz, "Variable Bandwidth Birefringent Filter for Tunable Femtosecond Lasers," IEEE J. Quantum Electron. **28**(10), 2142–2150 (1992).
19. U. Demirbas, G. S. Petrich, D. Li, A. Sennaroglu, L. A. Kolodziejski, F. X. Kärtner, and J. G. Fujimoto, "Femtosecond tuning of Cr:colquiriite lasers with AlGaAs-based saturable Bragg reflectors," J. Opt. Soc. Am. B **28**(5), 986–993 (2011).
20. U. Demirbas, "Off-surface optic axis birefringent filters for smooth tuning of broadband lasers," Appl. Opt. **56**(28), 7815–7825 (2017).
21. U. Demirbas, R. Uecker, J. G. Fujimoto, and A. Leitenstorfer, "Multicolor lasers using birefringent filters: experimental demonstration with Cr:Nd:GSGG and Cr:LiSAF," Opt. Express **25**(3), 2594–2607 (2017).
22. S. D. Zhu, "Birefringent filter with tilted optic axis for tuning dye lasers: theory and design," Appl. Opt. **29**(3), 410–415 (1990).
23. X. L. Wang and J. Q. Yao, "Transmitted and tuning characteristics of birefringent filters," Appl. Opt. **31**(22), 4505–4508 (1992).
24. Q. W. Yin, H. D. Lu, and K. C. Peng, "Investigation of the thermal lens effect of the TGG crystal in high-power frequency-doubled laser with single frequency operation," Opt. Express **23**(4), 4981–4990 (2015).
25. C. W. Zhang, H. D. Lu, Q. W. Yin, and J. Su, "Continuous-wave single-frequency laser with dual wavelength at 1064 and 532 nm," Appl. Opt. **53**(28), 6371–6374 (2014).
26. W. Z. Wang, H. D. Lu, J. Su, and K. C. Peng, "Broadband tunable single-frequency Nd:YVO4/LBO green laser with high output power," Appl. Opt. **52**(11), 2279–2285 (2013).
27. H. D. Lu, J. Su, and K. C. Peng, "Study on intracavity losses and output coupler transmission of all-solid-state tunable Ti:Sapphire laser," Chinese Lasers **37**(9), 2328–2333 (2010).
28. X. J. Sun, J. Wei, W. Z. Wang, and H. D. Lu, "Realization of a continuous frequency-tuning Ti:Sapphire laser with an intracavity locked etalon," Chin. Opt. Lett. **13**(7), 071401–71404 (2015).
29. Y. H. Cha, Y. W. Lee, K. -H. Ko, E. C. Jung, G. Lim, J. Kim, T. -S. Kim, and D. -Y. Jeong, "Development of a 756 nm, 3W injection-locked CW Ti:sapphire laser," Appl. Opt. **44**(36), 7810–7813 (2005).
30. L. P. Zhang, G. L. Yin, F. Q. Li, Z. Shi, and H. D. Lu, "All-solid-state tunable Ti:sapphire Laser with high-power and single-frequency at 900 nm," Chinese Lasers **44**(12), 1201002 (2017).
31. H. L. Li, H. L. Xu, B. S. Yang, Q. D. Chen, T. Zhang, and H. B. Sun, "Sensing combustion intermediates by femtosecond filament excitation," Opt. Lett. **38**(8), 1250–1252 (2013).
32. F. Q. Li, H. J. Li, and H. D. Lu, "Realization of a tunable 455.5-nm laser with low intensity noise by intracavity frequency-doubled Ti:sapphire laser," IEEE J. Quantum Electron. **52**(2), 1–6 (2016).
33. F. Q. Li, B. Zhao, J. Wei, P. X. Jin, H. D. Lu, and K. C. Peng, "A continuously tunable single-frequency 455 nm blue laser for high-state excitation transition of cesium," Opt. Lett. **44**(15), 3785–3788 (2019).
34. P. X. Jin, H. D. Lu, Y. X. Wei, J. Su, and K. C. Peng, "Single-frequency CW Ti:sapphire laser with intensity noise manipulation and continuous frequency-tuning," Opt. Lett. **42**(1), 143–146 (2017).
35. C. Weiman and T. W. Hanch, "Doppler-free laser polarization spectroscopy," Phys. Rev. Lett. **36**(20), 1170–1173 (1976).
36. Y. Yoshikaw, T. Umeki, T. Mukae, T. Mukae, Y. Torii, and T. Kuga, "Frequency stabilization of a laser diode with use of light-induced birefringence in an atomic vapor," Appl. Opt. **42**(33), 6645–6649 (2003).

218.28.243.164 {ts '2021-02-17 19:20:21'}